EXPERIMENTAL ANALYSIS OF SHELL-LIKE DEPLOYABLE ANCHORS FOR INCREASED TENSILE RESISTANCE

Kaylee A. TUCKER[1] and Ann C. SYCHTERZ[2]

[1]Graduate student, Civil and Environmental Engineering, University of Illinois at Urbana-Champaign, 205 N Mathews Ave, Urbana, Illinois 61821, United States
152TuckerK@gmail.com
[2]PhD., Assistant Professor, Civil and Environmental Engineering, University of Illinois at Urbana-Champaign
asychter@illinois.edu

Editor's Note: Manuscript submitted 06 July 2023; revisions received 14 April and 10 July 2024; accepted 19 August 2024. This paper is open for written discussion, which should be submitted to the IASS Secretariat no later than Month 2025.

DOI: https://doi.org/10.20898/j.iass.2024.011

ABSTRACT

Structures with deployable and compliant mechanisms are new to the domain of underground geotechnical systems. An anchor with rotationally deploying compliant thin-wall elements has been developed. This paper presents variations of this anchor that are targeted to increase the surface area associated with the anchor. This increased surface area correlates to higher skin friction to better resist tensile forces. The number and sizing of the deployable components, called awns, are investigated. The work presented here includes methods to change the deployment behavior of the awns by changing the shape of the awns and by using functionally graded materials for increased resistance when the anchor is subjected to uplift forces. Test members were fabricated from a combination of flexible and rigid polymers via additive manufacturing. Experimental testing included anchor deployment tests and awn tension tests. For deployment tests, torque was applied to an anchor placed in clear sand. Awn tension tests provided additional information about the deformation of functionally graded awns through isolated testing of the awns. The presented design and experimental methodologies give insights into the behavior of small-scale deployable anchors.

Keywords: *Deployable, compliant, anchor, experimental validation, functionally graded materials*

1. INTRODUCTION

1.1. Background

Civil structures that change shape to address specific challenges such as transportation, installation, and effectiveness are new to the field of underground structures. A deployable compliant anchor, as described in this work, applies principles of shape-changing structures to improve the performance of ground anchors. Improving the performance of foundation systems will reduce the amount of material associated with them, addressing more sustainable practices in geotechnical engineering. Less material facilitates logistics and fuel associated with transportation as units can be more efficiently moved to remote installation locations offshore or on land. Additionally reduced are the energy associated with the system and its cost.

Deployable structures are a type of transformable structure that change shape from a compact state to an expanded state as their size increases [1], [2]. Deployable structures have potential for increased capacity and the ability to be stored in a smaller volume. In practice, many contemporary structures including scissor structures [2], [3] use rigid materials and preconnected parts for easier deployment. Flexible materials are often seen in deployable structures that only need to deploy once. This is common in space applications such as solar sails, solar arrays, and deployable spacecraft [4-6]. A combination of rigid and flexible materials used in deployable structures can be seen in examples like

deployable masts with flexible cables [7] and membrane-based space reflectors [8]. The use of deployable structures has been limited to aboveground and space structures but has not yet been extended to underground use.

Compliant structures change shape via elastic or plastic deformations. Compliant elements are monolithic elements that deform to perform their functions [9]. The mechanisms involved in these structures function with non-rigid joints and are flexible like natural elements [10]. While most structures are designed to be stiff and strong, the goal of compliant structures is to be flexible and strong, like those found in nature [11], [12]. Compliant mechanisms are monolithically cast [13], thus reducing the need for mechanical coupling and on-site assembly. This can facilitate constructability and installation. Additionally, with fewer parts, compliant mechanisms can be designed to be lightweight, which can decrease transportation requirements [11], [14]. Previous work has looked to nature for inspiration but has mainly focused on aboveground applications.

Ground anchoring systems—including piles—are underground foundation elements. These systems must resist compression due to gravity loads and tension due to uplift from wind or wave forces. Here are three types of anchors that have been widely installed – piles, suction caissons, and drag embedded anchors (DEAs). Piles are a flexible system that can withstand a wide variety of load conditions that other types of anchors may not be able to. Piles can take vertical and horizontal loads [15]. Drawbacks include their performance under horizontal loading [15], environmental effects [16], and cost [15]. While it depends on the specific context of the project, piles can be up to five times more expensive than DEAs (the least expensive type of these anchors). Despite these drawbacks, anchor piles are an advantageous system for foundations due to their versatility.

Existing work [15, 17-20] has been done in combining radial protrusions on anchors and in exploring systems that actively change shape during installation or operation. Helical piles, which are comprised of a pile with attached helical plates resist lateral and axial loads [15], [17]. Rigid fins positioned radially can also be installed in pipelines to better resist uplift loads when installed in sand [18]. Suction embedded plate anchors are a system that deploys into soil after installation [15], [19]. Piles that have anchor wings have also been explored. After a pile is rotated into sand, wings hinge outwards and provide improved resistance to uplift loads [20]. The combination of deployable and compliant systems—the latter of which changes shape and size elastically—has not yet been investigated for geotechnical engineering.

Both deployable and compliant structures can be observed in the internal structures of plants and animals [1], [21]. Often, natural structures have inherent flexibility and softness, like in unravelling leaves and blooming flowers [22]. In structural engineering, the folding mechanisms associated with leaves, petals, and insect wings have been modeled and applied in large-scale origami structures [23]. Large scale structural analogues to natural structures have approximated compliant mechanisms with origami structures, but compliant versions have not yet been developed.

In the field of geotechnical engineering, biologically-inspired anchor piles have also been developed. Some studies have focused on the geometry associated with the anchor piles and have taken cues from biological systems. Along this thread, static piles with snakeskin inspired geometries [24] and root-inspired anchor systems have been tested [25]. The axial load capacity of root-inspired anchor systems was compared against that of a conventional cylindrical pile of the same diameter. The lower bound of the ultimate load for the root-inspired anchor systems was more than twice that of the conventional pile. One drawback of this particular system is that it requires the attachment of bolts after installation [26]. Inspired by biological processes, these studies have focused on the geometry of anchor piles. However, these systems are static and rigid.

When changes in properties are closely matched with a part's function, its material can be considered a functionally graded material (FGM) [27]. These materials have properties that align with their function, which allows for material efficiency [28]. FGMs have been utilized for a wide range of applications including artificial ligaments, satellite antennas, helicopter components [29], and microfluidic valves [30]. At a larger, architectural scale, agricultural shading devices have been constructed using FGMs created from 3D-printed biopolymers [31]. However, FGMs have not yet been applied to large-scale structural or geotechnical systems.

The construction industry accounts for 30% of the global energy consumption including embodied energy from material extraction and production [32]. Civil engineering structures are generally overdesigned for most situations as they are designed to withstand worst-case scenarios, not their service loads [33], [34]. Geotechnical structures in particular face this issue. An analysis of 89 US projects found that more than 85% of the surveyed projects had inadequate site investigations [35]. On average, 0.3% of a project's cost is allocated to site investigations. Due to site-based uncertainties, geotechnical engineers overdesign their systems to reduce risk [35]. The potential reduction in carbon and material, along with the risk mitigation benefits of geotechnical systems that use compliant structures have received little attention.

The authors have previously developed a biologically inspired deployable compliant structure for geotechnical use [36-37]. This anchor is inspired by the deployment of cheatgrass seeds and is comprised of a static pile with deployable shell-like compliant attachments, called awns, that deform away from the pile. From this work, it was shown that the geometry of the awns influences shear resistance [36]. However, hammer-driven piles could have unintentional secondary effects, including noise pollution and damage to surrounding foundations. Although a preliminary design has been created [37], this anchor has not yet been experimentally tested under the action of torque-driven auger piles.

The objectives of this paper are:

1. Compare the role of multiple shell-like awns in terms of the force required to deploy the anchor.

2. Determine the role that awn thickness and height play in the deployability of the anchor.

3. Assess the function of awns with varied deployment patterns along their vertical axis for increased resistance when the anchor is subjected to uplift.

1.2. Limitations

This study provides a proof-of-concept for deployable compliant anchor piles at a small scale. Limitations of testing this anchor at a small scale include low effective stresses, boundary effects, and different deployment/installation methods from full-scale. At-scale challenges, such as the material for the anchor, the connections between the awn and the pile, and the installation of the anchor are not in the current scope of the study. Additionally, the anchors were tested in sand for this study – other types of soil will be tested in future work.

This work focuses on installation of the anchors – the actuation of the awns was measured, not the forces in the awns. For this reason, creep, a long-term effect, was not considered in the scope of the work. Plastic deformation was not directly measured, though it did occur. This type of deformation was outside of the scope of the work because it is a systemic issue and the work presented in this paper focuses on local, awn-specific effects.

Low effective stresses are not present in full-scale anchors or foundations. Boundary effects from the plastic plate and box used in the deployment tests are also present. The behavior of structural components is affected by soil properties – which is influenced by boundary effects. This study is focused on the behavior of the structure itself, but future work will need to address the limitations of the soil.

2. METHODOLOGY

2.1. Anchor Description

This research focuses on an anchor (Figure 1) that is comprised of a cylindrical pile and several compliant, shell-like attachments, called awns. These awns are radially arranged around the pile. The scope of this paper is to study deployment during installation; in-service loading is not within the scope of the paper. This work presents a solution to help with tensile forces that tend to be specific to the structure. Tension was of interest for this study as it relies on the surface of the anchor and soil strength. Resistance against compressive forces primarily focuses on anchor material and soil strength.

When the pile is rotated, the awns deploy into soil, which, in the case of this initial study, is sand. Due to their compliant nature, the awns deploy via bending. This change in shape and size increases the contact area between the awn and soil, increasing the total friction between the pile and the soil. Since surface friction between the anchor and soil resists tensile uplift forces, a deployment pattern that varies along the vertical axis of the awn increases the relative vertical projected area of the awn structure in the soil.

Anchors loaded in tension are of particular interest for this work. For example, anchors for systems

under cyclical loading, including offshore energy and marine systems, are loaded in tension. These large-scale systems require large anchors. Awn deployment has significant potential to increase tension capacity for a relatively small increase in material thanks to the increased friction between the pile and the soil. This is caused by the larger soil-structure contact area along the awns and a larger vertical projected area that leads to increased soil mobilization volume and shearing area.

The aim of this work is to develop an anchor that has both increased tensile resistance and lighter weight than conventional piles for efficient use of material. Additionally, this reduction in weight facilitates lower transportation costs to site, which presents a the largest potential benefit for remote regions such as offshore installations.

The anchors presented in this work are fabricated and tested at a small scale to perform a proof-of-concept study of the behavior of the system. Tests at full-scale, with appropriate construction materials, will be developed but are outside the scope of this paper.

The awns were developed using a parametric model [37]. This model provided control of the dimensions and arrangements of the awns. At this scale, the anchors were printed monolithically so the awn was smoothly attached to the pile. The models discussed in this paper are prototyped for a proof-of-concept investigation. Testing at larger scales is outside of the scope of this work.

2.2. Physical Fabrication

The tested anchors were fabricated on a Stratasys Objet500 Connex3 resin 3D printer. This multi-material printer has a build volume of 50 cm width, 40 cm length, and 30 cm depth. The machine prints layers of 25 μm and can combine materials to create a wide range of polymer materials that vary in rigidity and tensile strength (Table 1). Combined materials are comprised of two base resins that are simultaneously blended to create a hybrid material [38].

All test objects were fabricated using these materials. In all cases, the piles were printed in VeroMagentaV. This acrylic-like resin contrasted with VeroCyan, a similar material that was used for annotations. Combining VeroMagentaV, flexural strength of 75 MPa and a tensile strength of 50 MPa, and the rubber-like Agilus30, flexural strength of nearly zero and a tensile strength of 3.1 MPa. Calculation of the flexural strength of the material was possible through the volume of each material consumed in printing, thus having a weighted field strength of approximately 25 MPa and tensile strength of 9.3 MPa.

2.3. Awn Variations

All prototyped anchors feature a pile with a diameter of 25 mm and a height of 75 mm and at least one awn

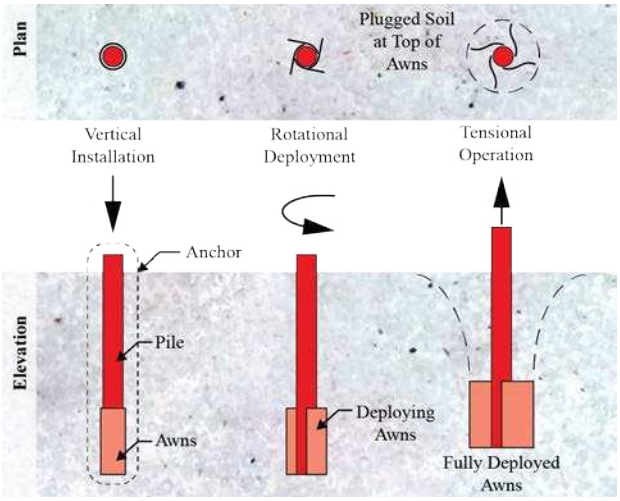

Figure 1: *Schematic illustration of anchor before, during, and after deployment.*

attached to the pile. The awns are defined by two connected arcs. The first arc is coincident with the profile of the pile and the second one has a larger radius. The profile of the awn is defined by a thickness parameter that gradually increases from the first arc to the second arc to smoothly attach the awn to the pile.

Table 1: *Polymer materials, compositions, and properties*

Material Name	**Material Composition**	**Tensile Strength**
VeroMagentaV	100% Acrylic-like resin; Fully rigid	65 MPa [39]
VeroCyan	100% Acrylic-like resin; Fully rigid	65 MPa [39]
Agilus30	100% Rubber-like resin; Fully flexible	3.1 MPa [40]
FLXA-MT-S95-DM-vivid	95% VeroMagentaV, 5% Agilus30; Semi-flexible	62 MPa

Three types of awn variations are explored in this paper: the number of awns, the dimensions of the awns, and the deployment behavior of the awns. The first type of variation explores the number of awns. Anchors with one, two, and three awns are generated

using the parametric model and fabricated using the method described in Section 2.2. These three cases were tested to understand the range of behavior between a minimum and maximum number of awns. Space constraints around the circumference of the pile—specifically related to the need for smooth attachment between the awn and the pile—limit the maximum number of awns at this scale to three awns.

In the next set of variations, the impact of awn dimensions on deployment is investigated. Although multiple parameters were used to define the exact shape of the awns, two parameters – awn height and awn thickness – are used to vary the size of the awn in this set of variations (Figure 2). Awn height (h_{awn}) is defined as the height of the awn in the Z direction. Awn thickness is gradually increased along the length of the awn, but for the purposes of this test, the reference thickness (t_{ref}) measured at the tip of the awn furthest from the connection to the pile is specified. All other parameters [37] are held constant in these models.

Four models are generated from a combination of two awn heights and two awn thicknesses. Awn heights are set at 15 mm and 35 mm to test two extrema. For testing purposes, an awn height of greater than 35 mm was not practical. The minimum height was determined by choosing a round number at least 50% less than the maximum.

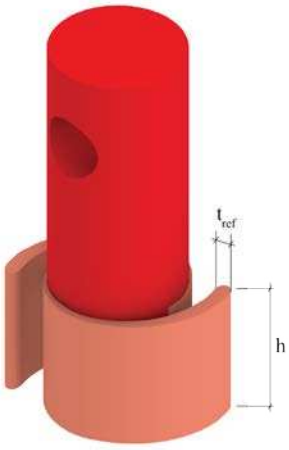

Figure 2: *Schematic illustration of anchor with the reference thickness (t_{ref}) and awn height (h) labeled.*

Two awn thicknesses are used in these tests: one set of anchors has awns with a reference thickness of 2.0 mm and the other has awns with 3.0 mm reference thickness. In previous test prints, awns with a reference thickness of under 2.0 mm buckled under testing. For the purposes of this work, awns with a reference thickness of 2.0 mm are used as a minimum.

The final type of awn variation considers changing the deployment behavior of the awns. In the awns developed earlier in this section, deployment behavior was consistent along the vertical (Z) axis. The next two variations are designed to allow the top portion of the awn to deploy more than the bottom (Figure 3). This would increase the projected surface area of the awns and improve their tensile resistance. Two methods for achieving this deployment behavior are proposed. The first method changes the overall geometry of the awn while the second changes the properties of the materials of the awn.

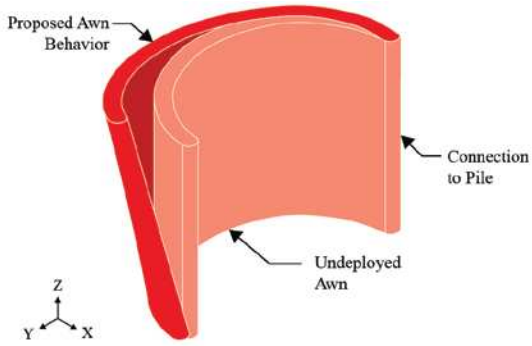

Figure 3: *Representation of proposed awn deployment behavior.*

The shape-based variation is an awn with a slanted connection to the pile (Figure 4). To construct this shape, the bottom footprint of this awn is copied to a point 25 mm in the positive Z direction. Next, it is rotated 42.5° in the XY plane. The bottom surface of the awn is defined by the original curve and the top surface of the awn is defined by the transformed curve. The two surfaces are connected by a third, doubly curved surface. Due to the rotation of the top surface of the awn, the interface between the awn and the pile is slanted at 20.5° from the Z axis.

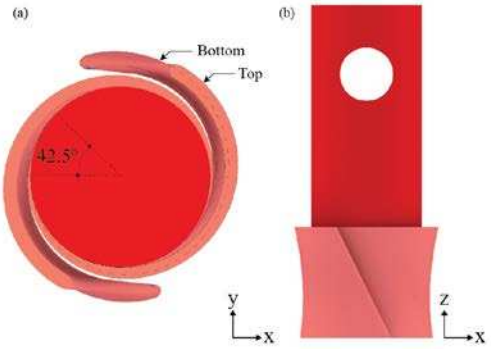

Figure 4: *Anchor with shifted and rotated awns shown in plan (a), with the top curve, bottom curve, and rotation angle marked and perspective (b).*

The second, material-based, variation of the awns explored functionally graded awns. Here, stiffer material is utilized at different points throughout the awn. The stiffer material in this experiment is VeroMagentaV (Table 1). FLXA-S95-DM-vivid, a semi-flexible material, is used in the other portions of the awn. Stiffer material is concentrated at the bottom of the awn to allow the top of the awn to deform more than the bottom. The grading patterns shown here are inspired by plant structures (Figure 5) and are transferred to the awn using a parametric definition [41].

Functionally-graded materials can be realized through various strategies. In this set of experiments, the cross-section was held constant to allow for future comparison with previously tested anchors. Stiffness is the primary parameter while the cross-section is held constant.

Figure 5: *Biologically inspired functionally graded materials applied to deployable anchor: anchor model (a); leaf, as inspiration (b); pattern applied onto awn (c).*

2.4. Experimental Setup

The anchors are tested by deploying them in Ranco-Sil™ B (30/50 mesh) fused silica sand [42] to determine the deployment of the awns. When the sand is mixed with sugar water (198 g sugar to 100 mL water) in a ratio of 42 g sugar water to 100 g sand, the resulting mixture becomes translucent. This clarity is important for data extraction. Sand was distributed evenly by hand. This experiment was conducted at 1g for the purposes of proof-of-concept. Therefore, the sand was not compacted and measured at this stage of work.

The median diameter (d50) of Ranco-Sil™ B is 0.52 mm [43]. This value is approximate and based on the product data sheet. For pile and shallow foundations, it is recommended that the ratio of the diameter of the foundation (D) divided by the median diameter of the sand (d50) should be greater than 30 [44], [45], [46]. D/d50 for the pile tested in this study is 48. For any stage of deployment, D/d50 will be greater than 30 and the effect of the grain size will be minimal.

The testing setup (Figure 6) is comprised of a clear acrylic box placed over a wooden crate on a table. An Inswan INS-1 document camera (a video camera with an adjustable arm) [47] is placed underneath the crate in a position in which the bottom of the acrylic box is visible. The anchor is placed inside the box with enough petroleum jelly sufficient to create a 1 mm thick layer between the pile and the bottom of the box. The sugar-sand solution is added around the anchor to fill the box to the top of the awns.

An acrylic plate with a hole in the center is added to ensure that the anchor stays in the center of the acrylic box. A nylon cord is threaded through a horizontal hole through the pile and is wrapped around the pile so that a coil is formed. Each side of the cord is laid on pulleys mounted on the edges of the wooden crate. The ends of the string are tied onto a measurement device under the table. When the measurement device is pulled downwards, the anchor rotates, and the awns deploy.

The purpose of this test is to understand the deployment of the awns. The resistance of the soil allows the awns to deploy as they rotate. In practice, the anchor would be drilled with an auger and then rotated in place to deploy. At this scale, the anchor is placed in the acrylic box and rotated.

The awn count tests are performed with a load cell as the measurement device. This device has a capacity of 4500 N and a resolution of 4.5 N. In all remaining experiments, a PASCO PASPORT High Resolution Force Sensor is utilized. This force sensor has a range of ±50 N and a resolution of 0.002 N. Testing found that the two devices produced similar results, but the PASPORT sensor was more sensitive than the load cell and had data acquisition benefits.

Functionally graded patterns are tested by performing tension tests on the awns alone. This test is necessary to understand the behavior of the top and the bottom of the awns. The deployment testing procedure described above focuses on extracting data from the bottom of the awn. An additional test was conducted to characterize the behavior at the top of the awn.

The test object for the functionally graded awn test is comprised of a modified awn. The awn footprint is extended to be tangent with the part of the awn that would be attached to the pile. Two holes with radii of 1.25 mm are added to the other end of the awn. For this test, the thickness of the awn is held constant along the length of the curve so that the pattern can

be analyzed independently from the thickness. The extended portion of the awn is clamped to a piece of plywood that is mounted off the edge of a table (Figure 7a) in alignment with the blue line shown in Figure 7b. Trackers are added to the edge of the awn to mark the start and end points of the curve. Cotton twine is threaded through the holes and the force sensor is attached to the twine.

A document camera is positioned so that the curved edge of the awn is visible. The tension tests are performed by instantaneously loading the awn with a force of 10 N, unloading it, and then repeating the process for a total of three tests. For all models, the tests are performed with a camera facing the top of the awn first. The process is repeated with the camera facing the bottom of the awn (Figure 7b).

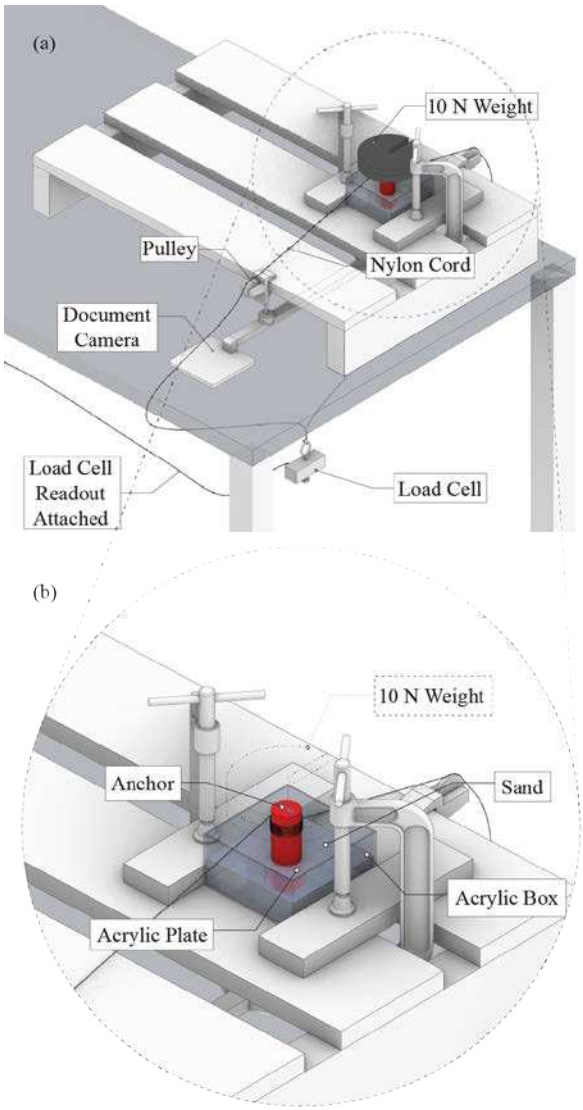

Figure 6: *Representation of deployment testing setup showing data collection methods (a) and anchor setup (b).*

For both the deployment and the tension tests, the video output and force output are synchronized to ensure that the force is known for any frame of the video. During testing, the video data is recorded by the native Windows Camera application and force data is recorded by PASCO Capstone software. Both windows are recorded with Open Broadcasting Software (OBS) Studio to ensure that the outputs could later be synchronized.

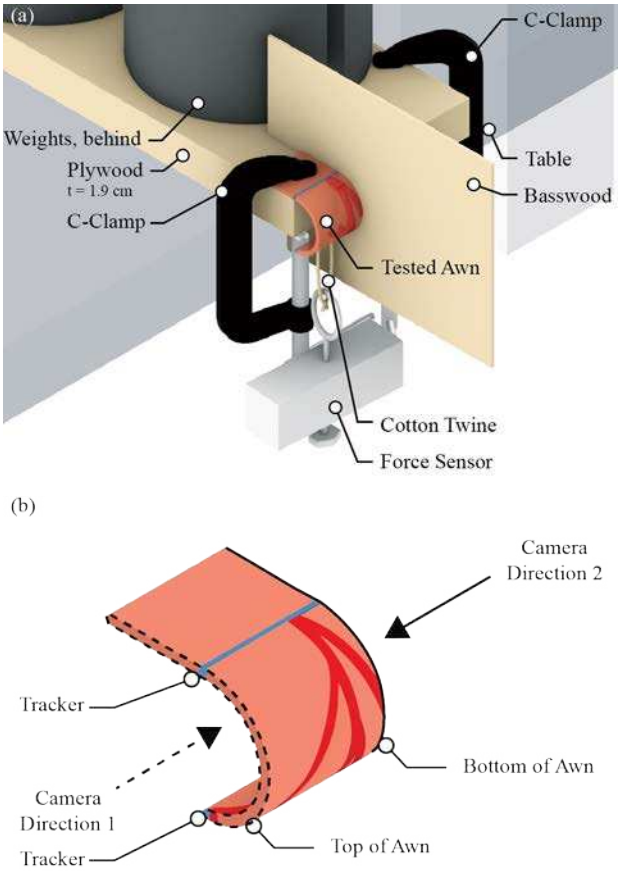

Figure 7**:** *Experimental testing for functionally graded awns showing tension test setup, with labels (a) and printed awns for testing, showing materials and parts (b).*

Data from the deployment tests is extracted by exporting two images of the deployment video – one before deployment and one at the maximum force. The forces at these frames are read from the synchronization video and noted. Each awn contains a set of position trackers embedded into the print in the VeroCyan material (Figure 8). A rotation tracker is also embedded into the pile.

In Rhinoceros 7, a 3D modeling software, distances between the position tracker located on the shell-like awn structure and the position tracker located on the pile are measured before and after deployment. This deployment distance is measured for each awn. The

change in angle between the pre-deployment and post-deployment rotation tracker is also found.

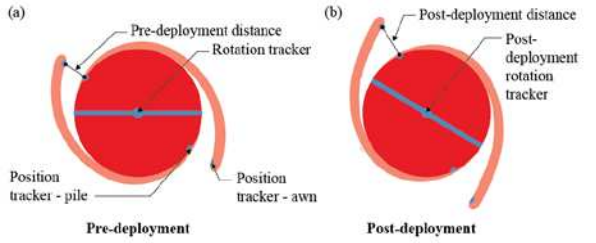

Figure 8: *Representation of trackers at pre-deployment (a) and post-deployment (b).*

A similar method is used for the tension tests. Images are extracted for the pre-deployment state and each post-deployment state – defined here as the first frame where a force is recorded above 10 N. The curves are traced in Rhinoceros 7 and an average curve is calculated for the three post-deployment states by finding the arithmetic mean of the three curves. The composite curve is compared to the unloaded curve and is discussed in Section 3.

3. RESULTS

3.1. Awn Count

In this experiment, anchors with one, two, and three awns were tested. The only varied parameter in these tests was the number of awns. Three samples of each iteration were fabricated and were tested twice using the load cell as the measurement device. Pre- and post-deployment images were extracted for each trial (Figure 9).

The maximum force was calculated as the average of the maximum force across all trials (Table 2). The test was stopped when the awns had deployed to a 90° angle with the pile. The rotation was calculated as the change in rotation between the pre-deployment anchor and the anchor at the maximum force, averaged across the trials. Awn deployment was calculated as an average of the deployment distances at the maximum force for all awns across all trials. The maximum force of each iteration was extracted to assess how anchors with more than one awn perform in comparison to a one-awn baseline.

The behavior of the system is dependent on the number of awns. The three-awn anchor deployed more than either the one-awn or two-awn anchor, but more force is required.

Adding awns increase the deployment force, but the effect is most evident when adding the second awn. When a second awn is added to a one-awn anchor, the force increases by 8.6 N. When adding a second awn to form a three-awn anchor, only a 4.3 N increase in the deployment force is measured.

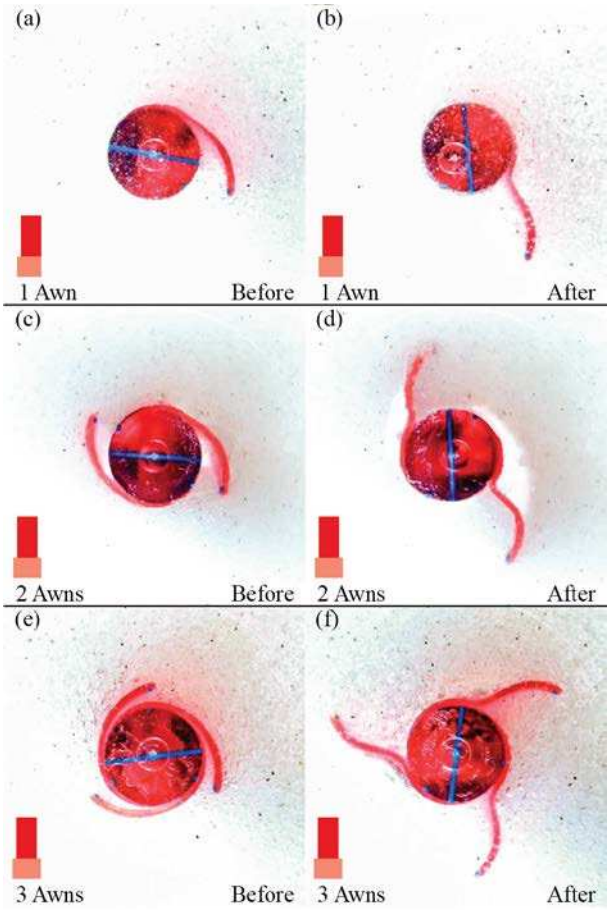

Figure 9: *3D printed anchor testing awn count shown at pre-deployment ((a), (c), (e)), and post-deployment ((b), (d), (f)).*

Table 2: *Average results at maximum force*

Awn Count	Rotation (°)	σ	Awn Deployment (mm)	σ
1	66.0	26.5	14.6	0.5
2	61.9	23.1	12.4	5.8
3	77.7	16.7	16.8	0.2

Awn Count	Maximum Force (N)	σ	Change from Awn Count1 Force (%)
1	12.2	3.4	0%
2	20.6	5.4	69%
3	23.4	4.8	92%

3.2. Awn Sizing

Four anchors were tested to determine how awn sizing affects deployment. As stated in Section 2.3, a

combination of two awn thicknesses and two awn heights forms the basis for these tests (Figure 10). All anchors were tested using the PASCO Force Sensor. The average force required to deploy the

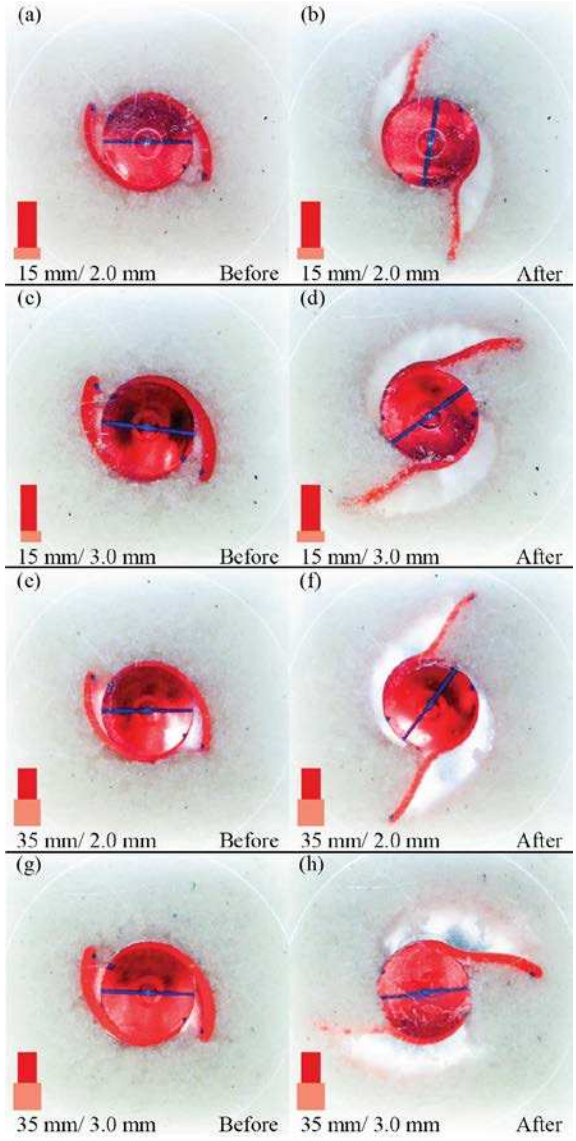

Figure 10: *3D printed anchor testing awn sizing shown at pre-deployment ((a), (c), (e), (g)), and post-deployment ((b), (d), (f), (h)).*

awns by a distance of 1 mm was calculated using awn deployment and maximum force measurements. These measurements were calculated using the same method as described in Section 3.1 (Table 3).

These results show that as the thickness of the awn increases, the force required to deploy the awn by a distance of 1 mm increases as well. The anchors with 3.0 mm thick awns require more force to deploy by the same distance as their 2.0 mm thick counterparts. Additionally, the increase in the average force to deploy the awns by a distance of 1 mm is greater when increasing the awn thickness than when increasing the awn height from 15 to 35 mm.

Table 3: *Average force (N) required to deploy awns by a distance of 1 mm.*

		Awn Thickness (mm)			
		2.0		**3.0**	
		Force (N)	σ	Force (N)	σ
Awn Height (mm)	15	0.55	0.01	1.37	0.04
	35	0.77	0.03	1.89	0.13

3.3. Deployment Behavior – Slanted Interface

An anchor with a slanted interface was tested to determine how a shape-based awn variation would change deployment behavior. This anchor, introduced in Section 2.3, was fabricated once and tested three times with the PASCO Force Sensor. The slanted-interface awn exhibits deployment behavior that is significantly different from the awns with vertical connections to the pile.

The slanted-interface awns have variable deployment along their height. In Figure 11, two trials are shown. In the first trial, called *Slanted Awn 1*, one awn deploys more than the other. The blue dashed line indicates that the bottom of the awn deploys less than the top of the awn. This effect is more evident in *Slanted Awn 3*, the third trial.

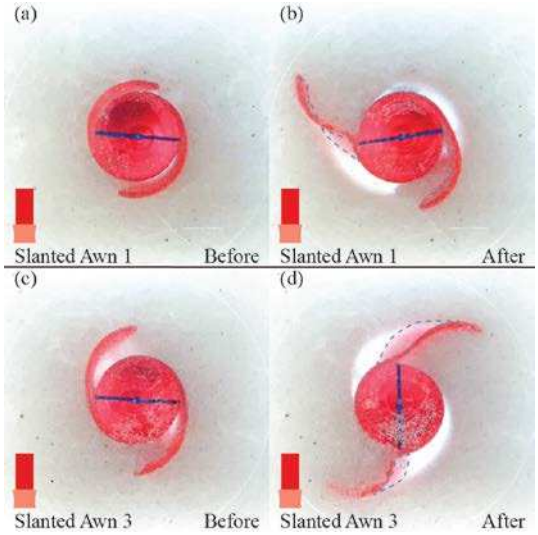

Figure 11: *3D printed anchor testing slanted connection awn – two trials, with out-of-plane bending outlined in blue shown at pre-deployment ((a), (c)), and post-deployment ((b), (d)).*

After the three trials were performed, the awns remained deformed. The top edge of the awn deformed more than the bottom edge of the awn when load was applied evenly (Figure 12a).

It was also observed that the attachment interface between the awn and pile after deployment was curved instead of slanted (Figure 12b). Both the top and the bottom of the awn deployed, but the amount of deployment was greater at the top, arising from the curved Z-axis profile of this awn. This phenomenon was not noted in the awns tested with vertical attachment interfaces.

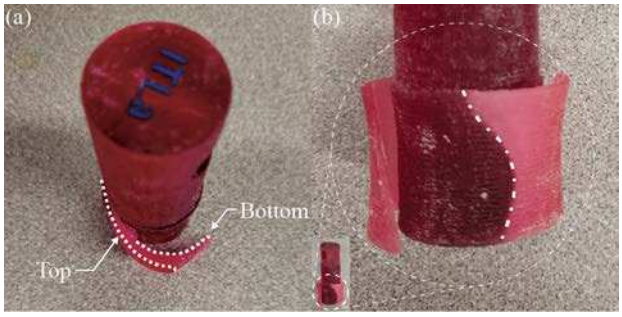

Figure 12: *3D printed anchor after testing slanted connection awn in bird's-eye view – showing deformed awn shape in thick dashed line (a) and elevation – showing awn-pile interface in thick dash-dot line (b).*

3.4. Deployment Behavior – Functionally Graded Awns

Twelve patterns and an additional non-FGM awn (*nFGM*) were all printed once and tested with the method explained in Section 2.4. These patterns were determined by sampling the design space for a breadth and depth of models.

The profiles of the awns before deployment – shown in blue – and after deployment – shown in pink – were compared (Figure 13, 14). The small icons to the right of each header are representations of the tested patterns. The *nFGM* awn did not contain any of the rigid material, VeroMagentaV. The percent elongation of the awns was calculated in the X-axis and Y-axis and was compared across the twelve patterns (Table 4, 5).

The *nFGM* awn has the most elongation in both the X-axis and Y-axis directions. Although isotropic behavior was expected, the high flexibility of FLXA-MT-S95-DM-vivid causes the awn to remain deformed after the first trial of this test.

Pattern a is a symmetrically designed awn and shows the same percent Y-axis elongation on the top and bottom of the awn. *Pattern d* and *pattern e* both

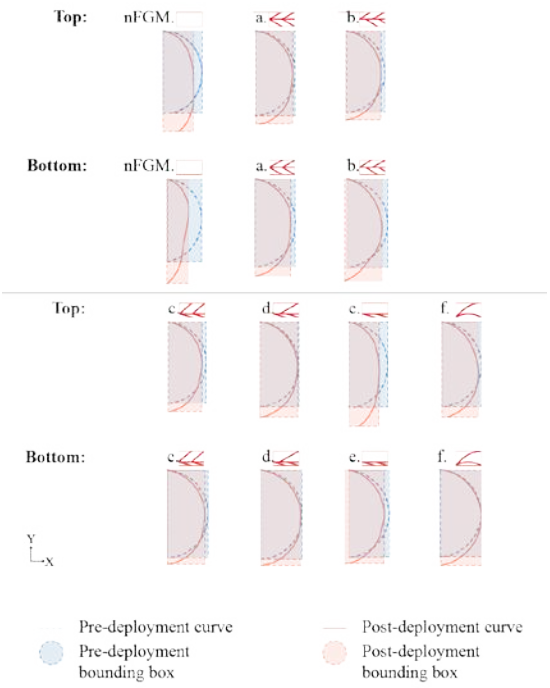

Figure 13: *Awn profiles for the nFGM awn and pattern a through pattern f from top and bottom shown pre-deployment (blue) and post-deployment (pink).*

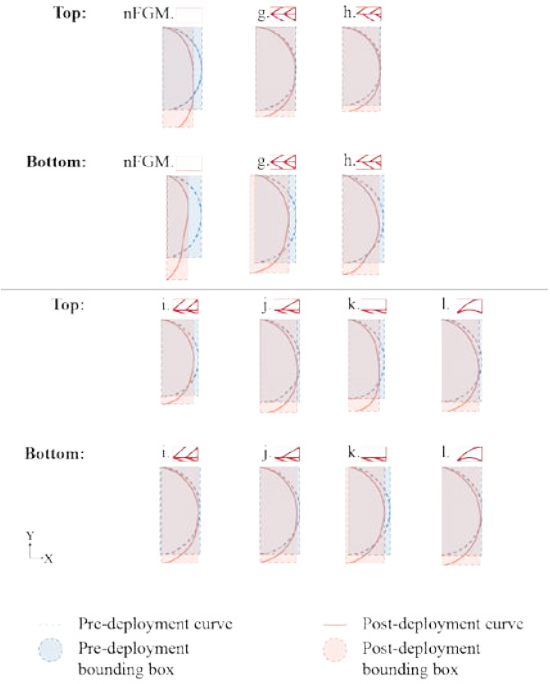

Figure 14: *Awn profiles for the nFGM awn and pattern g through pattern l from top and bottom shown pre-deployment (blue) and post- deployment (pink).*

show similar percent X-axis and Y-axis elongation for the bottom of the awn. However, *pattern e* has much higher percent elongation in the X-axis and Y-axis in the top of the awn. The difference between these two

patterns is the amount of rigid material in the top half of the awn. *Pattern d*, the awn with a lower percent elongation at the top of the awn, has more rigid material present in that area than *pattern e*.

Table 4: *Percent Y-axis elongation of awn profiles for the nFGM awn and pattern a through pattern l.*

	nFGM	*a*	*b*	*c*	*d*	*e*
Top	22%	10%	10%	10%	13%	22%
Bottom	27%	10%	15%	8%	7%	8%

f	*g*	*h*	*i*	*j*	*k*	*l*
13%	7%	8%	10%	13%	16%	12%
10%	12%	13%	10%	9%	10%	11%

Table 5: *Percent X-axis elongation of awn profiles for the nFGM awn and pattern a through pattern l.*

	nFGM	*a*	*b*	*c*	*d*	*e*
Top	-21%	-8%	-8%	-12%	0%	-23%
Bottom	-37%	-13%	-8%	-7%	-3%	-3%

f	*g*	*h*	*i*	*j*	*k*	*l*
-7%	-3%	-3%	-13%	-7%	-14%	-7%
-3%	-6%	-12%	-9%	-9%	-7%	-5%

The vertical strip of material present in *pattern g* through *pattern l* generally decreases the percent elongation along the Y-axis so that the top half of the awn deforms less than the bottom. However, this did not happen in *pattern k,* the pattern which contained no rigid material in the top half of the awn except for the 2 mm strip of material that formed the vertical strip. A decrease in percent Y-axis elongation is still seen for this pattern compared to the version without the vertical strip, *pattern e*.

4. DISCUSSION – EMBODIED ENERGY

4.1. Awn Count

For the tests conducted, adding awns correlates with increased deployment force, as discussed in Section 3.1. The interaction between the awns in anchors with more than one awn likely contributed to the non-linear increase in deployment force. The sand is displaced by each awn during deployment - when more awns are added, the amount of sand deformed per awn decreases due to the interaction between awns.

As the goal of this experiment was in showing that the awns deployed in prototype models, the focus was on the comparison between pre-deployment and post-deployment geometry. This proof-of-concept was targeted to the mechanism of deployment and was experimentally tested. Continuous tracking of the position of the awns will be the focus of future work.

A material analysis was carried out on the three tested awn arrangements along with a baseline pile without awns (Figure 15). This analysis is exclusively focused on material usage of anchors. It does not consider their deployment force or stress capacity. When increased capacity is required for anchor piles, friction is increased by increasing the surface area of piles. If the diameter of the anchor were increased, the drilling rig to install the anchor to the same depth would need to be more powerful. Increasing the height of the pile to increase surface area presents practical geotechnical and on-site challenges that are beyond the scope of this work.

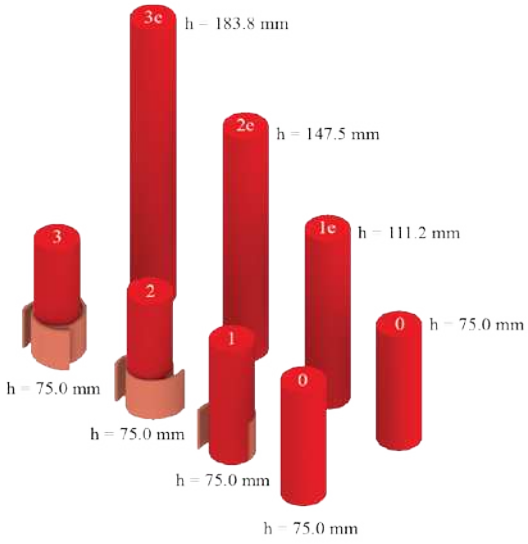

Figure 15: *Material analysis of tested anchors and their pile-only counterparts.*

Comparing the designed anchors and equivalent piles with identical surface areas, it is possible to compare the material usage of the two systems. The surface area of each anchor was calculated in Rhinoceros 7 and a pile with an equivalent surface area and radius was generated.

The volume of each anchor and equivalent pile was calculated and compared (Table 6). Through this analysis, it was determined that an anchor comprised of deployable compliant awns attached to a cylindrical pile uses less material than an equivalent anchor pile with the same surface area. Changing the radius of the pile is also possible but is less materially efficient because volume increases exponentially with radius.

While all the anchors are more materially efficient than their pile-only counterparts, adding each awn makes this effect more pronounced. A one-awn anchor provides a 29% reduction in material in comparison to a pile-only system with identical surface area. For a two-awn anchor, this reduction increases to 44% and for a three-awn anchor, the reduction in material is 53%. The difference in the material reduction effect is largest between a one-awn system and a two-awn system.

Table 6: *Surface area and volume for tested anchors and equivalent piles.*

Type	Radius (mm)	Height (mm)	Surface Area (cm^2)	Volume (cm^3)
Baseline	12.5	75.0	69	37
1 Awn Anchor	12.5	75.0	97	39
1 Awn Pile-Only Equivalent	12.5	111.2	97	55
2 Awn Anchor	12.5	75.0	126	40
2 Awn Pile-Only Equivalent	12.5	147.5	126	72
3 Awn Anchor	12.5	75.0	154	42
3 Awn Pile-Only Equivalent	12.5	183.8	154	90

Regardless, the increase in deployment force should be considered in combination with the volume of material used, the practicalities of construction, and the specific soil conditions in question. The deployment force is an indicator of the ease of installation but may also be a predictor for tensile capacity. Figure 16 illustrates the conceptual relationship between required force and displacement.

When awns are difficult to deploy, they also may be difficult to pull out of soil – increasing the tensile capacity of the anchor. A higher deployment force – which may predict higher tensile capacity – can be helpful. However, it may not be feasible to install an anchor that has an extremely high deployment force. A deployment force that is excessively low would not provide any resistance benefits. Balancing the requirement for high tensile capacity with the feasibility of deploying the awns in a construction environment could be achieved with a two-awn anchor, which provides a trade-off between resistance and amount of material used.

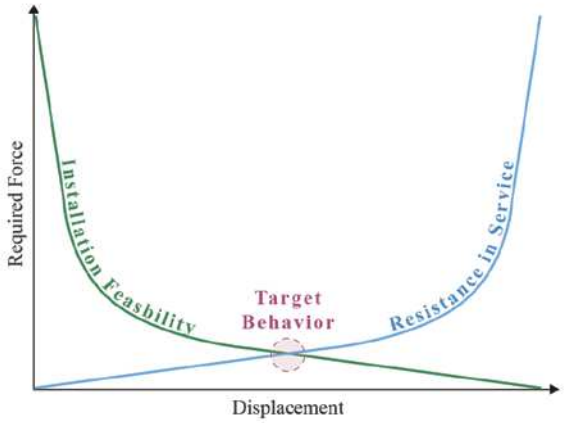

Figure 16: *Representation of relationship between required force and displacement, showing resistance in service (blue), installation feasibility (green), and target behavior (pink).*

4.2. Awn Sizing

Sizing the awns depends on the context in which the anchor will be used. Factors that should be considered include soil properties, ease of installation, embodied energy, and tensile capacity. Awn height and awn thickness both positively correlate with required deployment force. However, these two parameters affect the surface area and material volume differently.

Varying the height and thickness of the awn affects the surface area and volume. Comparing these properties to the deployment force can provide a design space to understand how different anchors can provide different properties (Figure 17). The decision as to whether awn thickness, awn height, or both should be increased depends on the aims of the anchor in question.

Increasing both the awn thickness and height of the awn will increase the surface area of the anchor at the expense of increased material volume, as can be seen in the *35 mm/ 3.0 mm* model, which has a 35 mm tall awn and a thickness of 3.0 mm. Balancing the two parameters can provide additional

possibilities. Although this change is slightly materially inefficient, it may be desirable for installation purposes to only increase awn thickness due to its large effect on deployment force. On the other hand, it may be necessary to maximize the surface area to increase the tensile capacity. Increasing the awn height is a materially efficient way to accomplish this. Varying both parameters can generate a system with hybrid properties and can produce awns like the *35 mm /2.0 mm* model that balance maximizing surface area, minimizing volume, and maximizing deployment force.

4.3. Deployment Behavior – Slanted Interface

A material analysis was also performed on the awns with slanted interfaces. The surface area and volume were compared between a two-awn anchor with slanted interface awns and a two-awn anchor with vertically aligned interface awns (Table 9).

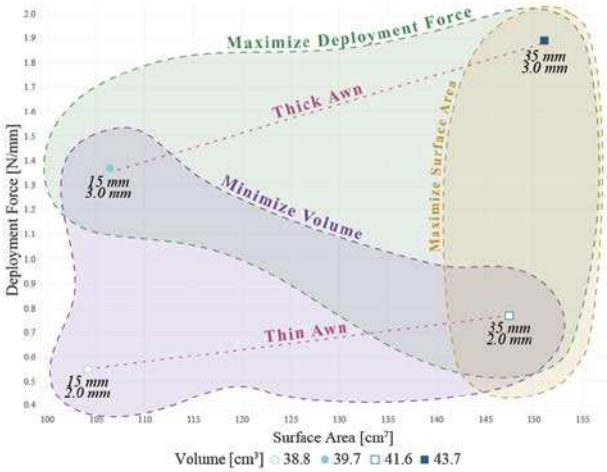

Figure 17*: *Performance and characteristics of awns with labels showing heights and thicknesses. X-axis shows surface area, Y-axis shows deployment force, symbols denote volume.

The surface area of the slanted awns is significantly higher than that of the vertically aligned awn – with only a slight increase in volume. This increase in surface area, related to a curved Z-axis profile, produces natural bending. A slanted awn anchor has a higher surface area than a vertically aligned awn anchor, increasing tensile capacity without increasing material.

4.4. Deployment Behavior – Functionally Graded Awns

Functionally graded awns with different patterns feature different deformations. Additionally, awns with asymmetrical patterns show different deformations for the top and the bottom of the awn. Concentrating rigid material at the bottom of the awn increases the stiffness of that portion of the awn and allows the top of the awn to deform more. This can be beneficial as the projected surface area would increase, improving the awn performance.

***Table 9:** Surface area and volume for slanted-interface awn and vertically aligned interface awn.*

	Surface Area (cm^2)	**Volume** (cm^3)
Slanted interface	145	41
Vertically aligned interface	126	40

5. CONCLUSION

The conclusions of this paper are:

1. A two-awn arrangement can provide a trade-off between factors including deployment force, material, and ease of installation.

2. Both increasing the thickness and increasing the height of the shell-like awn structures increase the deployment force of the anchor, but sizing requirements depend on specific use cases.

3. Awns with varied deployment patterns along their vertical axis successfully deform in a scoop-like shape when tested in isolation. When applied to the anchor, this deformation creates a scoop-like shape which increases the projected geometry in the direction of force. This combines the conclusions of this work with the authors' previous work for effectiveness of vertical awns of hammer-driven piles.

ACKNOWLEDGMENTS

Support from the National Science Foundation (CMMI_2207296), the University of Illinois at Urbana-Champaign, and the State of Illinois are gratefully acknowledged. Testing assistance from Richard Yoo is also appreciated.

REFERENCES

[1] S. Pellegrino, *Deployable Structures*. Wien-New York: Springer Verlag, 2001. (DOI: 10.1007/978-3-7091-2584-7)

[2] Y. Akgün, C. J. Gantes, W. Sobek, K. Korkmaz, and K. Kalochairetis, "A novel adaptive spatial scissor-hinge structural mechanism for convertible roofs,"

Engineering Structures, vol. 33, no. 4, Art. no. 4, Apr. 2011, (DOI: 10.1016/j.engstruct.2011.01.014).

[3] C. J. García-Mora and J. Sánchez-Sánchez, "Actuation methods for deployable scissor structures," *Automation in Construction*, vol. 131, p. 103894, Nov. 2021, (DOI: 10.1016/j.autcon.2021.103894).

[4] H. Furuya, "Concept of Deployable Tensegrity Structures in Space Application," *International Journal of Space Structures*, vol. 7, no. 2, pp. 143–151, Jun. 1992, (DOI: 10.1177/026635119200700207).

[5] G. Tibert, "Deployable Tensegrity Structures for Space Applications," *Royal Institute of Technology*, 2002. (DOI: 10.2514/6.2003-1978)

[6] J. Block, M. Straubel, and M. Wiedemann, "Ultralight deployable booms for solar sails and other large gossamer structures in space," *Acta Astronautica*, vol. 68, no. 7, Art. no. 7, Apr. 2011, (DOI: 10.1016/j.actaastro.2010.09.005).

[7] G. Tibert and S. Pellegrino, "Deployable Tensegrity Masts," presented at the 44th AIAA/ASME/ASCE/AHS/ASC Structures, Structural Dynamics, and Materials Conference, Apr. 2003. (DOI: 10.2514/6.2003-1978).

[8] L. Datashvili, H. Baier, E. Wehrle, T. Kuhn, and J. Hoffmann, "Large Shell-Membrane Space Reflectors," in *51st AIAA/ASME/ASCE/AHS/ASC Structures, Structural Dynamics, and Materials Conference; 18th AIAA/ASME/AHS Adaptive Structures Conference; 12th*, Orlando, Florida: American Institute of Aeronautics and Astronautics, Apr. 2010. (DOI: 10.2514/6.2010-2504).

[9] L. L. Howell, S. P. Magleby, and B. M. Olsen, *Handbook of compliant mechanisms*. Chichester, West Sussex, United Kingdom Hoboken, New Jersey: John Wiley & Sons, Inc, 2013. (DOI: 10.1002/9781118516485)

[10] S. Kota, J. Joo, Z. Li, S. M. Rodgers, and J. Sniegowski, "Design of Compliant Mechanisms: Applications to MEMS," *Analog Integrated Circuits and Signal Processing*, vol. 29, no. 1, pp. 7–15, Oct. 2001, (DOI: 10.1023/A:1011265810471).

[11] S. Kota and G. K. Ananthasuresh, "Designing compliant mechanisms," *Mechanical Engineering-CIME*, vol. 117, no. 11, Art. no. 11, Nov. 1995.

[12] M. Frecker, "Synthesis through Topology Optimization," in *Handbook of Compliant Mechanisms*, John Wiley & Sons, Ltd, 2013, pp. 93–107. (DOI: 10.1002/9781118516485.ch7).

[13] L. Zentner and V. Böhm, "On the Classification of Compliant Mechanisms," in *Proceedings of EUCOMES 08*, M. Ceccarelli, Ed., Dordrecht: Springer Netherlands, 2009, pp. 431–438. (DOI: 10.1007/978-1-4020-8915-2_52).

[14] L. L. Howell, "Introduction to Compliant Mechanisms," in *Handbook of Compliant Mechanisms*, John Wiley & Sons, Ltd, 2013, pp. 1–13. (DOI: 10.1002/9781118516485.ch1).

[15] C. Aubeny, *Geomechanics of Marine Anchors*. Boca Raton: CRC Press, 2017. (DOI: 10.4324/9781351237376).

[16] A. Colaço, P. Alves Costa, C. Mont'Alverne Parente, and A. Silva Cardoso, "Ground-borne noise and vibrations in buildings induced by pile driving: An integrated approach," *Applied Acoustics*, vol. 179, p. 108059, Aug. 2021, (DOI: 10.1016/j.apacoust.2021.108059).

[17] Y. V. S. N. Prasad and S. N. Rao, "Lateral Capacity of Helical Piles in Clays," *Journal of Geotechnical Engineering*, vol. 122, no. 11, Art. no. 11, Nov. 1996, (DOI: 10.1061/(ASCE)0733-9410(1996)122:11(938)).

[18] J. Tom, C. O'Loughlin, D. White, A. Haghighi, and A. Maconochie, "The effect of radial fins on the uplift resistance of buried pipelines," *Géotechnique Letters*, vol. 7, Mar. 2017, (DOI: 10.1680/jgele.16.00142).

[19] B. Wilde, H. Treu, and T. Fulton, "Field Testing of Suction Embedded Plate Anchors," presented at the The Eleventh International Offshore and Polar Engineering Conference, OnePetro, Jun. 2001.

[20] M. Sakr, A. Nazir, W. Azzam, and A. Sallam, "Model study of single pile with wings under uplift loads," *Applied Ocean Research*, vol. 100, p. 102187, Jul. 2020, (DOI: 10.1016/j.apor.2020.102187).

[21] J. Lienhard, S. Schleicher, and J. Knippers, "Bio-inspired, Flexible Structures and Materials," in *Biotechnologies and Biomimetics for Civil Engineering*, F. Pacheco Torgal, J. A. Labrincha, M. V. Diamanti, C.-P. Yu, and H. K. Lee, Eds., Cham: Springer International Publishing, 2015, pp. 275–296. (DOI: 10.1007/978-3-319-09287-4_12).

[22] J. F. V. Vincent, "Deployable Structures in Biology," in *Morpho-functional Machines: The New Species*, F. Hara and R. Pfeifer, Eds., Tokyo: Springer Japan, 2003, pp. 23–40. (DOI: 10.1007/978-4-431-67869-4_2).

[23] D. Baerlecken, R. Gentry, M. Swarts, and N. Wonoto, "Structural, Deployable Folds — Design and Simulation of Biological Inspired Folded Structures," *International Journal of Architectural Computing*, vol. 12, no. 3, Art. no. 3, Sep. 2014, (DOI: 10.1260/1478-0771.12.3.243).

[24] K. B. O'Hara and A. Martinez, "Monotonic and Cyclic Frictional Resistance Directionality in Snakeskin-Inspired Surfaces and Piles," *Journal of Geotechnical and Geoenvironmental Engineering*, vol. 146, no. 11, p. 04020116, Nov. 2020, (DOI: 10.1061/(ASCE)GT.1943-5606.0002368).

[25] A. Martinez *et al.*, "Bio-inspired geotechnical engineering: principles, current work, opportunities and challenges," *Géotechnique*, vol. 72, no. 8, Art. no. 8, Aug. 2022, (DOI: 10.1680/jgeot.20.P.170).

[26] S. A. Aleali, P. Bandini, and C. M. Newtson, "Multifaceted Bioinspiration for Improving the Shaft Resistance of Deep Foundations," *J Bionic Eng*, vol. 17, no. 5, Art. no. 5, Sep. 2020, (DOI: 10.1007/s42235-020-0076-6).

[27] N. Oxman and J. L. Rosenberg, "Material-based Design Computation An Inquiry into Digital Simulation of Physical Material Properties as Design Generators," *International Journal of Architectural Computing*, vol. 5, no. 1, Art. no. 1, Jan. 2007, (DOI: 10.1260/147807707780912985).

[28] K. Dierichs and A. Menges, "Functionally Graded Aggregate Structures: Digital Additive Manufacturing With Designed Granulates," presented at the ACADIA 2012: Synthetic Digital Ecologies, San Francisco (California), USA, 2012, pp. 295–304. (DOI: 10.52842/conf.acadia.2012.295).

[29] T. Khan, "State of the art review of Functionally Graded Materials," May 2019, (DOI: 10.1109/ICOMET.2019.8673489).

[30] S. J. Keating, M. I. Gariboldi, W. G. Patrick, S. Sharma, D. S. Kong, and N. Oxman, "3D Printed Multimaterial Microfluidic Valve," *PLOS ONE*, vol. 11, no. 8, Art. no. 8, Aug. 2016, (DOI: 10.1371/journal.pone.0160624).

[31] J. M. Lesna and P. Nicholas, "De gradus - Programming heterogeneous performance of functionally graded bio-polymers for degradable agricultural shading structures.," presented at the CAADRIA 2020: RE:Anthropocene, Bangkok, Thailand, 2020, pp. 383–392. (DOI: 10.52842/conf.caadria.2020.2.383).

[32] International Energy Agency, "Buildings," IEA, Paris, 2022. [Online]. Available: https://www.iea.org/reports/buildings

[33] A. P. Reksowardojo, G. Senatore, A. Srivastava, C. Carroll, and I. F. C. Smith, "Design and testing of a low-energy and -carbon prototype structure that adapts to loading through shape morphing," *International Journal of Solids and Structures*, vol. 252, p. 111629, Oct. 2022, (DOI: 10.1016/j.ijsolstr.2022.111629).

[34] A. P. Reksowardojo and G. Senatore, Eds., "Design of ultra-lightweight and energy-efficient civil structures through shape morphing," *Computers & Structures*, 2023, (DOI: 10.1016/j.compstruc.2023.107149).

[35] M. B. Jaksa, W. S. Kaggwa, G. A. Fenton, and H. G. Poulos, "A framework for quantifying the reliability of geotechnical investigations," 2003.

[36] A. C. Sychterz, I. Bernardi, J. Tom, and R. Beemer, "Nonlinear soil-structure behavior of a deployable and compliant anchor system," *Canadian Journal of Civil Engineering*, 2021. (DOI: 10.1139/cjce-2021-0204)

[37] K. Tucker and A. C. Sychterz, "Analyzing Geosystems with Deployable Compliant Mechanisms for Enhanced Tension Capacity," *Proceedings of the Canadian Society of Civil Engineering Annual Conference 2022,* 2024. (DOI: 10.1007/978-3-031-34027-7_32)

[38] "PolyJet Multi-Material -Technical Application Guide," Stratasys.

[39] Stratasys, "Vero Material Data Sheet," Stratasys. [Online]. Available: https://stratasysstorage01.file.core.windows.net/ssys-websites-files-prod/Public1/Materials/Polyjet/Vero%20Family%20(Rigid)/Vero%20Family%20-%20EN%20Data%20Sheet%20PolyJet%20Material.pdf?sv=2017-04-17&sr=f&sig=T7J4HP%2FJKo2O8Pl3U350YFJfJ%2BfI%2BmDaHpdpiYQmbf0%3D&st=2022-08-27T14%3A11%3A05Z&se=2023-08-28T14%3A11%3A05Z&sp=rwl

[40] Stratasys, "Agilus30 Material Data Sheet," Stratasys. [Online]. Available: https://www.stratasys.com/siteassets/materials/materials-catalog/polyjet-materials/agilus30-colors/mds_pj_agilus30_cmy_0422a.pdf?v=4991e7

[41] A. C. Sychterz and K. A. Tucker, "Comparison of biologically inspired functionally graded deployable geosystems with experimental measurements," *Proceedings of IASS Annual Symposia*, vol. 2023, no. 20, pp. 1–12, Oct. 2023.

[42] "Ransom & Randolph," ransom-randolph. [Online]. Available: https://www.ransom-randolph.com/ranco-sil

[43] "Ranco-Sil Fused Silica Product Data Sheet," Ransom & Randolph. [Online]. Available: https://www.ransom-randolph.com/_files/ugd/cc5f22_42cd5e5f05684ce3bffa428b5a3602cb.pdf

[44] [. Fioravante, "On the Shaft Friction Modelling of Non-Displacement Piles in Sand," *Soils and Foundations*, vol. 42, no. 2, pp. 23–33, Apr. 2002, (DOI: 10.3208/sandf.42.2_23).

[45] J. Garnier *et al.*, "Catalogue of scaling laws and similitude questions in geotechnical centrifuge modelling," *International Journal of Physical Modelling in Geotechnics*, vol. 7, no. 3, pp. 01–23, Sep. 2007, (DOI: 10.1680/ijpmg.2007.070301).

[46] M. D. Bolton *et al.*, "Centrifuge cone penetration tests in sand," *Géotechnique*, vol. 49, no. 4, pp. 543–552, Aug. 1999, (DOI: 10.1680/geot.1999.49.4.543).

[47] "INS-1 Document Camera." INSWAN, 2023. [Online]. Available: https://www.inswan.com/en/INS-1